Computers and Electronics in Agriculture 168 (2020) 105142

Contents lists available at ScienceDirect

Computers and Electronics in Agriculture

journal homepage: www.elsevier.com/locate/compag

Accuracy and precision evaluation of two low-cost RTK global navigation satellite systems

Domingos Sárvio Magalhães Valente[a,1], Abdul Momin[b,1], Tony Grift[b,*], Alan Hansen[b,*]

[a] Department of Agricultural Engineering, Federal University of Vicosa (UFV), Brazil
[b] Department of Agricultural and Biological Engineering, University of Illinois at Urbana-Champaign, 1304 West Pennsylvania Avenue, Urbana, IL 61801, USA

ARTICLE INFO

Keywords:
Precision agriculture
GPS data
Single-frequency
Field robotics

ABSTRACT

Two low-cost Real-time Kinematic Global Navigation Satellite Systems (RTK GNSSs) being the Emlid “Reach RTK” and the NavSpark “NS-HP” were evaluated in terms of positioning accuracy and precision. Each GNSSs’ rover unit was mounted on a field robot that travelled by manual remote control along a pre-defined test track in six repeated trials. The precision of the two systems was evaluated through F-test statistics.

The combined accuracy of the two GNSSs was determined by comparing the positioning data to a fixed known distance between the GNSS antennas on the robot (472 mm). In three out of six trials, both GNSSs remained in fixed solution status, and showed a Root Mean Square Error (RMSE) of less than 50 mm, which was within the expected range. In two other trials, one of the GNSSs started in float solution status, and subsequently transitioned to fixed solution status. In these trials, the RMSE was still well within one meter, which was expected in float solution status. In one trial, a false fixed position status was encountered, where the NavSpark GNSS falsely claimed it was in fixed solution status. This issue needs to be alleviated in the future by improvements in signal conditioning, noise, and software, and/or by sensor fusion. Although the Emlid GNSS had superior localization performance, as its percentage of data in fixed solution status was 94.0% compared to 71.5% for the NavSpark GNSS, both were deemed promising for use on experimental field robots.

1. Introduction

Precision Agriculture (PA) comprises an information and technology-based management system to collect, identify, and analyse spatial variability within fields. Its goals are to optimize farm profitability and sustainability, in addition to protecting the environment. Spatial information technologies include the Global Positioning System (GPS), Geographical Information Systems (GIS), Variable-Rate Technologies (VRT), and Remote Sensing (RS). The use of PA technologies can lead to increased efficiency in resource use, reduced environmental impact, increased food security, as well as improved quality of life and health of workers (Perez-Ruiz et al., 2012).

To obtain and manage spatial information within PA, the Global Navigation Satellite System (GNSS) is vital. In addition to the classical use of GNSS for agricultural machine tracking and guidance, currently, field robots and unmanned aerial vehicles (UAVs) are in widespread use in PA (Bakker et al., 2011; Bechar and Vigneault, 2017, 2016; Ji et al., 2012; Mousazadeh, 2013; Oksanen and Backman, 2013; Yin and Noguchi, 2013).

Agricultural field robots typically navigate between plant rows to perform a specific task (Bechar and Vigneault, 2017; Ji et al., 2012; Mousazadeh, 2013). UAVs acquire aerial imagery of agricultural fields with a resolution of approximately five centimetre per pixel. Since UAVs capture images that represent a large portion of the field, they can operate using low-cost GNSS devices with a positioning error of less than five meters. However, field robots operate within a limited space between crop rows and under varying soil conditions (Dong et al., 2013), and hence, require higher accuracy and precision than UAVs. Various guidance systems are in use in field robots such as GNSS based guidance (Bakker et al., 2011; Dong et al., 2013, 2011), vision based guidance (Morimoto et al., 2005; Xue et al., 2012; Yin and Noguchi, 2013), LIDAR based guidance (Weiss and Biber, 2011), and combinations of these (Subramanian et al., 2006). Field robot guidance based on GNSS uses real-time kinematic GNSS (RTK GNSS) that provides centimetre or sub-meter level error in real time (Bakker et al., 2011; Becharand Vigneault, 2017). RTK GNSS relies on wireless communication between a stationary base station and a mobile rover, the latter being typically affixed to an agricultural machine or robot (Dong et al., 2011;

* Corresponding authors.
E-mail address: grift@illinois.edu (T. Grift).
[1] First and second authors contributed equally to this manuscript.

https://doi.org/10.1016/j.compag.2019.105142
Received 26 August 2018; Received in revised form 10 November 2019; Accepted 29 November 2019

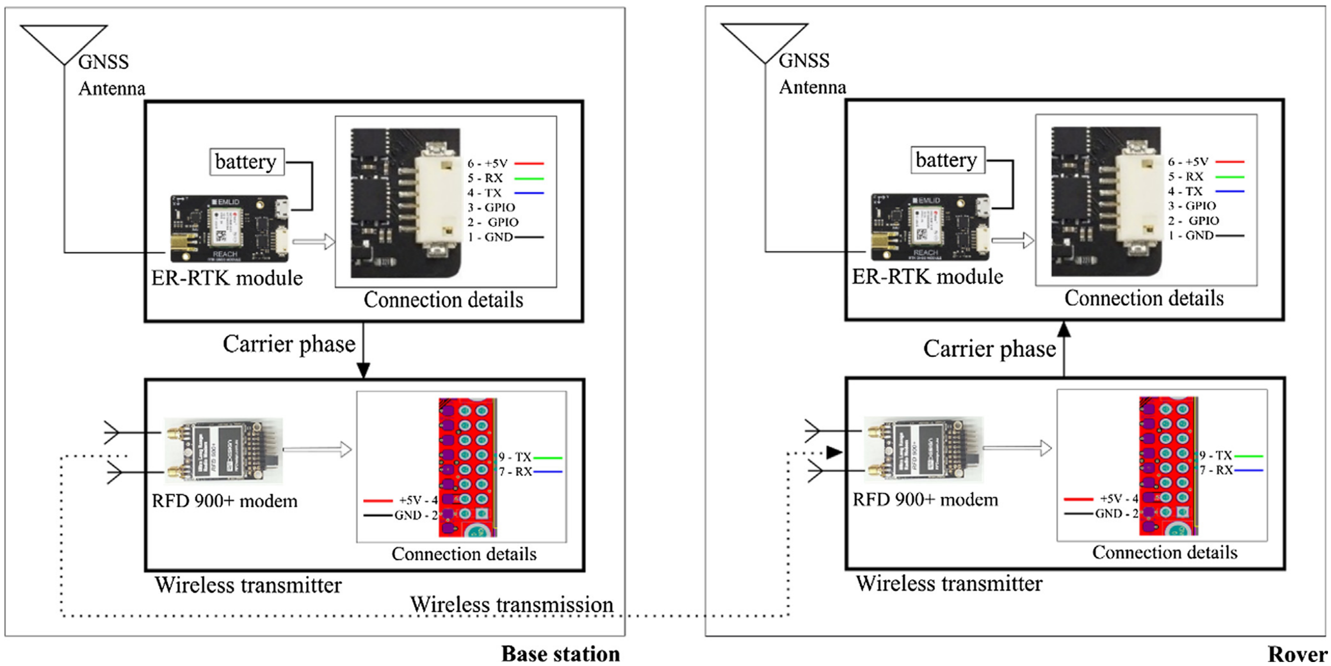

Fig. 1. Layout of the low-cost RTK GNSS comprising a base station and rover using Emlid Reach RTK modules (ER-RTK) and RFD 900 + modems for wireless communication.

Table 1
Emlid Reach RTK GNSS configuration.

Parameters	Rover	Base station
Mode	Kinematic	Base station
Elevation mask	15°	15°
Signal-to-noise ratio (SNR)	35 dB	35 dB
Update rate for positioning	5 Hz	5 Hz
Communication between rover and base station	Serial (RTCM 3)	Serial (RTCM 3)
Baud rate for serial communication	38,400 bps	38,400 bps
Integer ambiguity resolution (AR) for GPS	Fix and hold	Fix and hold
Positioning output format	Lat, lon	Lat, lon

Koo et al., 2017). The assumption is made that the positioning error occurring at the base station GNSS affects the rover's GNSS identically. Thus, a highly accurate rover position can be obtained by transmitting in real-time the positioning error from the base station to the rover. In an RTK GNSS, to obtain a "fixed" solution, with centimetre level accuracy and precision, at least five satellites need to be accessible to the base station and the rover simultaneously. A "float" solution, with a sub-meter level error, requires access to at least four satellites (Dabove and Manzino, 2017). In RTK GNSS, a carrier phase, sent from the satellites to the GNSS receivers, allows for positioning with high precision and accuracy. The carrier phase measurement is an integer number of cycles plus a fraction of a cycle. For the system to work properly, it is necessary to determine the integer number of cycles between a satellite and the GNSS receiver, a process termed integer ambiguity resolution.

Integration of a RTK GNSS in a robot or machine increases its cost dramatically (Dong et al., 2011; Mousazadeh, 2013; Pedersen et al., 2006), as RTK GNSSs can cost up to 20–30 thousand USD (Koo et al., 2017). Therefore, to widely proliferate the application of PA in general, and agricultural robotics in particular, it is imperative that the costs of RTK GNSS systems be reduced significantly (Mousazadeh, 2013). Low-cost, compact RTK GNSS modules are available that can be readily incorporated into robotic applications (Liu and Li, 2017; Odolinski, 2017; Odolinski and Teunissen, 2017; Tsakiri et al., 2017), since open source libraries are available for RTK GNSS correction (Takasu and Yasuda, 2009), and because system software can be executed on small, low-cost computer boards such as the BeagleBone Black and Raspberry Pi. The combination of these elements may enable wide-spread utilization of low-cost RTK GNSS technology in agriculture and beyond.

The objective of this research was to compare the positioning accuracy and precision of two low-cost, single-frequency RTK GNSS systems in a dynamic setting.

2. Materials and methods

The RTK GNSS modules tested were a "Reach RTK" (ER-RTK) manufactured by Emlid (Emlid Ltd, 2018) and a "NS-HP" (NS-RTK) manufactured by NavSpark (NavSpark, 2018). The ER-RTK module was based on the Ublox Neo-M8T single-frequency carrier phase GNSS chipset, featuring 72 channels, and supporting GPS/QZSS/ L1 C/A, GLONASS G1, BeiDou B1, SBAS L1 C/A, and Galileo E1. This module uses an Intel® Edison computer module integrated in a Ublox GNSS chipset which supports storage, processing, data transfer and wireless communication.

The ER-RTK uses open source RTK processing software named RTKLib (Takasu et al., 2009; Takasu and Yasuda, 2013, 2009) for processing raw data collected from a base station and rover for position correction. The RTKLib library allows for setting configuration parameters such as elevation mask, signal-to-noise ratio, communication baud rate, and integer ambiguity resolution. The ER-RTK uses a Tallysman TW4721 GNSS antenna, featuring low noise (1 dB), a gain of 26 dB, and the ability to receive L-band GPS, GLONASS, Beidou, and Galileo signals (L1, G1, B1, B1 BOC, B12, E1) as well as augmentation signals (WAAS, EGNOS and MSAS SBAS). To communicate between a base station and a rover, the ER-RTK modules were connected to an RFD 900 + modem using a serial UART port. Fig. 1 shows the layout of the RTK GNSS using ER-RTK modules and an RFD 900 + modem.

The ER-RTK module has a web-based application called ReachView to access the RTKLib library configuration, and others user settings. The base station's serial messages sent to the rover were 1002 (GPS L1 observations) and 1006 (ARP station coordinates). The setting parameters of the rover and base station configuration for RTKlib in ER-RTK are shown in Table 1.

The NS-RTK module is based on the SkyTra chipset, featuring 20

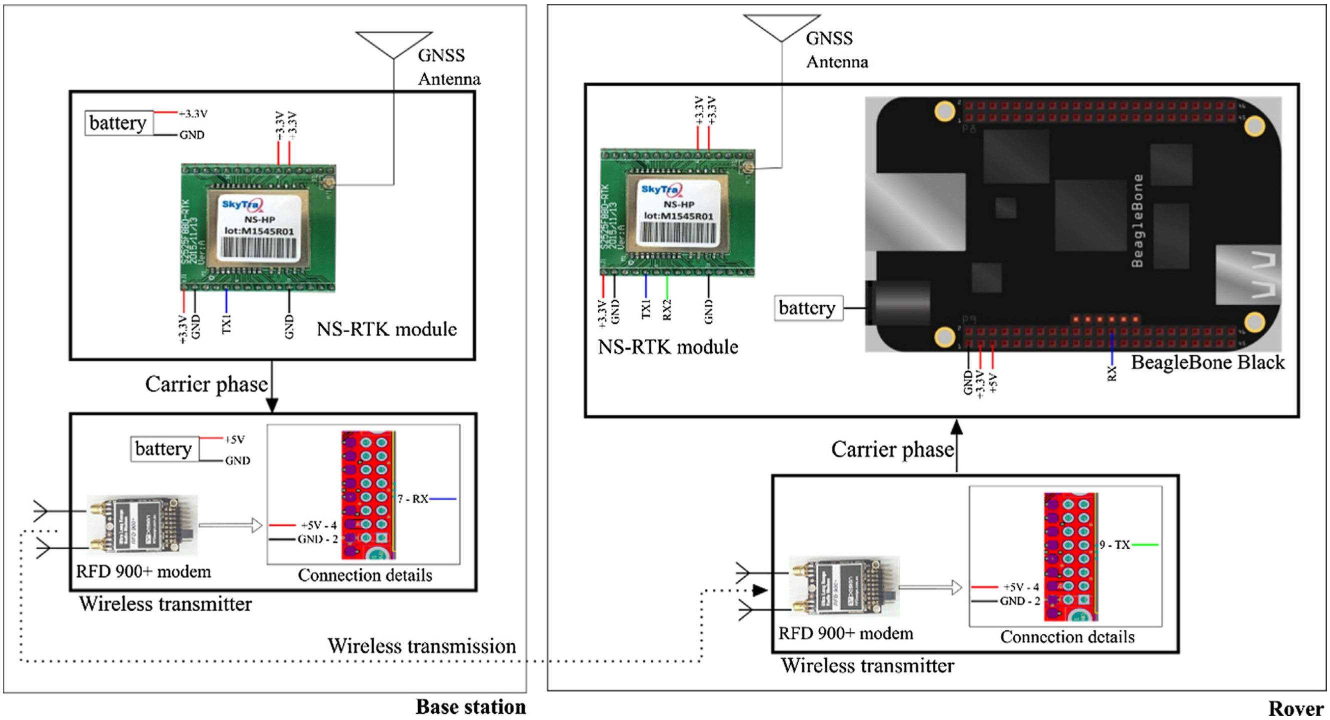

Fig. 2. Layout of low-cost RTK GNSS composed of NavSpark RTK modules (NS-RTK), whilst using RFD 900+ modems for wireless communication between base station and rover. The BeagleBone Black computer board was used to read and store data.

Table 2
NavSpark NS-HP RTK GNSS configuration.

Parameters	Rover	Base station
Mode	Kinematic	Base station
Elevation mask	15°	15°
Signal-to-noise ratio (SNR)	35 dB	35 dB
Update rate for positioning	1 Hz	1 Hz
Communication between rover and base station	Serial (RTCM 3)	Serial (RTCM 3)
Baud rate for serial communication	57,600 bps	57,600 bps
Positioning output format	NMEA 0183	NMEA 0183

GPS/SBAS/QZSS channels and 6 BDS channels, 1 Hz RTK, and single-frequency carrier phase (L1/B1 C/A Code) for RTK reception. The NS-RTK module firmware is stored in two 32-bit controllers, which process raw data from the base station and the rover to calculate corrections. The antenna used with the NS-RTK was a Tri-band GPS/Galileo/Beidou/Glonass active unit, operating at a frequency from 1558 MHz to 1615 MHz, noise of 2 dB, and a gain of 27 dB. A BeagleBone Black computer board (BBB) was connected to the NS-RTK rover module through a serial UART to read and store output correction data using Python code. Both NS-RTK modules were connected to a RFD 900+ modem through a serial UART port to allow communication between the base station and the rover. Fig. 2 shows the layout of the RTK GNSS using NS-RTK modules and RFD 900+ modem.

The NS-RTK modules were configured through a serial connection using GNSS Viewer Customer Release V2.0.296 software. Table 2 shows the settings for rover and base station for the NS-RTK firmware.

In the base station NS-RTK module, the output raw data was transmitted serially in RTCM3 format at a baud rate of 57,600 bps. The base module streamed 1002 (GPS L1 observations) and 1006 (ARP station coordinates) messages using the RTCM3 format. Communication between the base station and the rover was established through telemetry as shown in Figs. 1 and 2. For each RTK GNSS, the telemetry system comprised dual long-range RFD 900+ modems, with a range of 40 km depending on antennas and ground station control setup. The RFD modems were configured to operate at 915 MHz with transfer rates of 64 kBs^{-1}, a serial UART baud rate of 57,600 bps, with four 915 MHz, 3 dB dipole antennas (two for each modem).

The accuracy of any GNSS can be evaluated by evaluation of absolute errors, i.e., the distances between a current position and a reference position, whereas the precision can be evaluated by calculating the standard deviation of a set of recorded positions (Valbuena et al., 2010). To evaluate the performance of the two RTK GNSSs, experiments were conducted in which both modules were mounted on an agricultural robot. Base stations were mounted on a tripod as shown in Fig. 3. To reduce the probability of multipath error and interference, provide shielding and improve signal reception, the GNSS antennas were mounted on an aluminium ground plane.

The ER-RTK and the NS-RTK rovers were affixed to opposite sides of a robot (Fig. 4). The robot was based on a four-wheel-drive surface mobility platform (Gears Educational Systems, DEPCO, LLC, Pittsburg, KS). The overall length, width and height of the robot chassis was 610 × 610 × 330 mm, weighing 8.16 kg. During experimentation, the robot was remote controlled. To avoid interference and multipath errors, the antennas were mounted on 100 mm × 100 mm aluminium ground planes. The horizontal distance between the GNSS antennas was 472 mm. The unmarked antenna shown in Fig. 4 on the right was not used in this experiment.

Field tests were conducted on a grass surface, located at approximately lat/lon: 40.102239, −88.227140. The weather was clear with an ambient temperature of approximately 15 °C. A track marked with flags was used to conduct six dynamic experiments. The robot was moved along the track using human operated remote control and therefore approximately followed the same track repeatedly. For each trial, the robot started at the same position and travelled along the track with an average speed of 0.325 m s^{-1}. Before commencing an experiment, the robot was kept stationary for about five minutes, allowing both RTK GNSSs to fix their locations. The two base stations were located in the centre of the track at a mutual distance of approximately two meters.

The precision and accuracy were measured in a dynamic setting. To

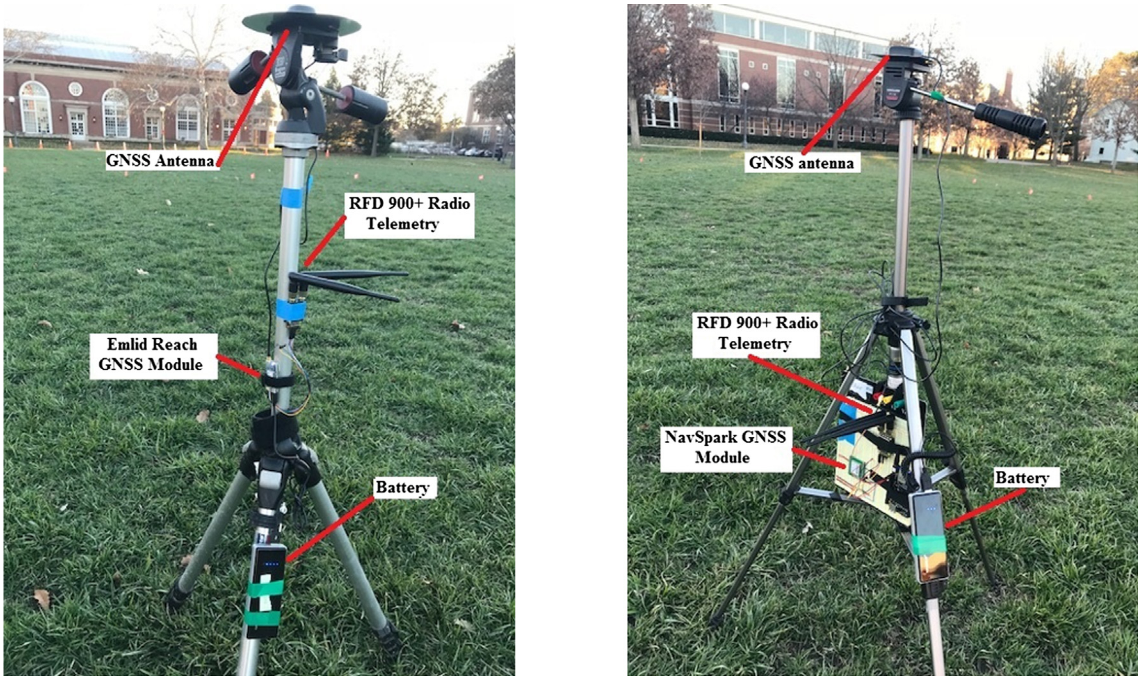

Fig. 3. Base station with Emlid Reach RTK (ER-RTK) module (left) and NavSpark RTK (NS-RTK) module (right).

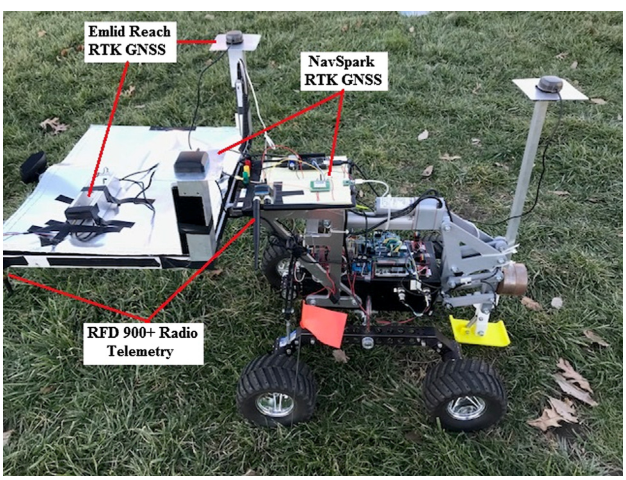

Fig. 4. Rover RTK GNSS module setup on the field robot.

evaluate the precision of the positioning data, a statistical analysis was conducted using distances through which the robot travelled during time intervals of one second, termed Distance Travelled Per Second (DTPS), as shown in Fig. 5. The mean, standard deviation (SD), minimum, maximum, and coefficient of variation (CV) for the DTPS data were calculated for both the ER-RTK and NS-RTK GNSSs. The analysis was conducted using open source GIS software (QGIS version 2.1815). In addition, to compare the precision between the two RTK systems, the Total Distance Travelled (TDT) was calculated, as the sum of the DTPSs for each of the six experiments. The SD of DTPS and TDT was mainly considered for explaining and comparing their level of precision. A statistical F-test was used to compare the SD of the TDT for each RTK GNSS.

Owing to the unavailability of a higher accuracy RTK system for comparison, the accuracy of the RTK GNSSs was determined by taking the fixed distance between the RTK antennas (472 mm, see Fig. 5) as a reference. As before, at second long time intervals, the Distance from the ER-RTK to the NS-RTK antenna (DEN) was calculated. The absolute dynamic error was considered the absolute difference between the reference distance of 472 mm and the recorded distance (DEN). Therefore, the calculated accuracy represents both RTK GNSSs combined. The mean, standard deviation, minimum, and maximum DEN were calculated. Then, the absolute dynamic errors for each second interval were calculated. Finally, the mean absolute distance error (MAE) and root-mean-square distance error (RMSE) of the DEN were calculated using Eqs. (1) and (2) respectively.

$$RMSE = \sqrt{\frac{\sum_{i=1}^{n}(DEN - 472)^2}{n}} \tag{1}$$

$$MAE = \frac{\sum_{i=1}^{n}|DEN - 472|}{n} \tag{2}$$

where DEN is the recorded distance in mm between the ER-RTK and the NS-RTK GNSS antennas, 472 in mm is the fixed physical distance between the ER-RTK and NS-RTK GNSS antennas, and n is the number of observations.

3. Results and discussion

The positioning data collected among six trials are shown in Fig. 6. In the figure, dots represent the ER-RTK GNSS, and crosses the NS-RTK GNSS. The ER-RTK and NS-RTK trajectories do not overlap because of the fixed distance between the GNSS antennas (472 mm). The carrier phase, sent from the satellites to GNSS receiver, is an integer number of cycles plus a fraction of a cycle. In RTK GNSS systems, algorithms are used to determine the exact number of cycles between receiver and satellites, a process termed integer ambiguity resolution, which allows to determine the distance between the receiver and satellites with high accuracy. A fixed solution is present when an integer ambiguity resolution is obtained, otherwise, a float solution is present. In the fixed solution case, potentially centimetre accuracy can be obtained (Dabove and Manzino, 2017). In Fig. 6, fixed and float solutions are represented in black and blue respectively.

In trial 1 (Fig. 6A) the ER-RTK GNSS from the start attained and maintained a fixed solution, implying that the GNSS receiver tracked and applied differential corrections to fix the phase ambiguities to an integer value. However, during the same test, the NS-RTK data were observed as float solutions, where ambiguity resolution resulted in a

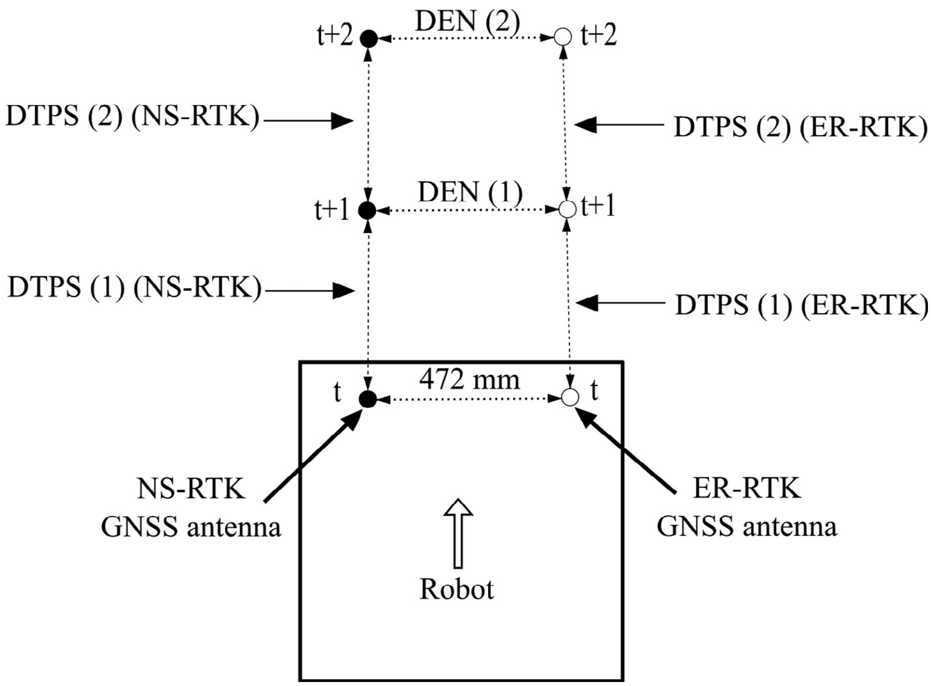

Fig. 5. Layout of the precision and accuracy measurement in a dynamic setting. DEN(i) denotes two data points representing the distance from the ER-RTK to the NS-RTK antenna for a second long time interval (i). The true value of this fixed distance was 472 mm. DTPS(i) denotes data points representing the distance through which the robot travelled during the same second long time interval (i).

decimal number. In the case of float solution, sub-meter accuracy is achievable (Dabove and Manzino, 2017). Although there was a float solution for the NS-RTK unit, the robot followed the predefined path with sub-meter accuracy, albeit with a higher offset error (difference between the calculated distance between the GNSS antennas and the true 472 mm) compared to the ER-RTK.

In trial 2 (Fig. 6B) the ER-RTK was initially in float solution and then graduated to a fixed solution, as shown in the zoomed-in portion of Fig. 6B, where the ER-RTK position status changed from a float (blue) to a fixed solution (black). 61.4% of the ER-RTK GNSS data was in fixed solution status whereas fixed solution status was observed for the NS-RTK along the entire track. It is clear that at the point where the position status of the ER-RTK GNSS changed from float to fixed solution, the offset distance between them reduced and the accuracy improved.

During trial 3 (Fig. 6C), trial 4 (Fig. 6D), and trial 6 (Fig. 6F), all data for both the ER-RTK and the NS-RTK were observed in fixed solution status.

In trial 5 (Fig. 6E) 98.7% of the ER-RTK data was in fixed solution status, and 63.4% of the NS-RTK data was in fixed solution status. Trial 5 is of particular interest since, as is clear from Fig. 6E, at the start of the trial, the observed coordinates of the NS-RTK GNSS were located far away from the track. The phenomenon observed here is termed a false fixed solution, meaning that the NS-RTK GNSS reports a fixed position solution (as shown with black crosses), while it is not. The false fixed solution phenomenon can happen for several reasons, among which erroneous estimation of phase ambiguities by the algorithm, noise in the correction data from the base station, and the effect of the environment in which the GNSS operates (Dabove and Manzino, 2017). Detecting false fix problems in single-frequency GNSS receivers is a challenge for future work. Dabove and Manzino (2017) used an artificial neural network (ANN) for detecting false fixed solutions for single-frequency GNSS receivers. Their algorithm had a 99.7% probability of detecting phase ambiguity in false fixed solution scenarios. In trial 5 (Fig. 6E), after some false fixed solution status data at the start, the NS-RTK data status transitioned to a float solution (zoomed in portion on the left), and eventually to fixed solution data (zoomed-in portion at the bottom). The percentages of data that were in fixed solution during all six trials combined was 94.0% for the ER-RTK GNSS and 71.5% for the NS-RTK GNSS. Therefore, overall, the ER-RTK GNSS yielded better results than the NS-RTK GNSS.

Table 3 shows the statistical analysis for Distances Travelled Per Second (DTPS) as described earlier and shown in Fig. 5. The coefficient of variation (CV), which represents the standard deviation divided by the mean, is an indicator of the relative precision of the DTPS data. A low CV value indicates precise data since the standard deviation around the mean is small (ideally zero). Table 3 shows that only for trial 1, the standard deviation was, based on an F-test, near identical for both RTK GNSSs. However, in this trial, the CV was the highest among all trials, in the range of [51.11, 53.2%]. Table 3 also shows that the CV values for both systems show consistency for trials 2, 3, 4 and 6. The CVs in trial 5 are consistent with trials 2, 3, 4, 6 for the ER-RTK GNSS (13.64%), but the CV for the NS-RTK GNSS is extreme (76.7%). This was caused by the effects of the false fixed solution issue as described earlier.

The CVs for the ER-RTK GNSS were consistently below 15% for all trials, except trial 1. The reason was that during trial 1 the robot was stopped for a few seconds, resulting in the minimum distance travelled being approximately 0.0 m (Table 3). The standard deviations of the NS-RTK GNSS data were greater than those of the ER-RTK GNSS for all trials according to an F-test at a 1% significance level. For trial 5, the differences were high compared to the other trials.

For further comparison, the Total Distance Travelled (TDT) was calculated for each RTK GNSS as shown in the right hand column of Table 3. While ignoring trial 5, which suffered from ample erroneous data, the TDT values among the two GNSSs showed a bias of on average 2.865 m. This was expected, since the ER-RTK antenna travelled outside and the NS-RTK inside the track.

Ideally, if both GNSSs had the same precision, they should have same standard deviation values. However, it was observed that the TDT standard deviation was significantly different between the RTK GNSSs, among all trials. Whilst taking all trials into account, the ER-RTK had a far lower standard deviation in the Total Distance Travelled (SDTDT = 356.31 mm) compared to the NS-RTK (SDTDT = 4411.12 mm), but this difference was influenced disproportionately by trial 5, which suffered from inconsistencies in the data. When trial 5 is not taken into account, the standard deviations in the Total Distance Travelled were found similar between the NS-RTK and the ER-RTK GNSS systems being 366.84 mm and 368.03 mm respectively (Table 3). However, the overall performance of the ER-RTK was deemed superior over the NS-RTK, as 94% of its data was obtained

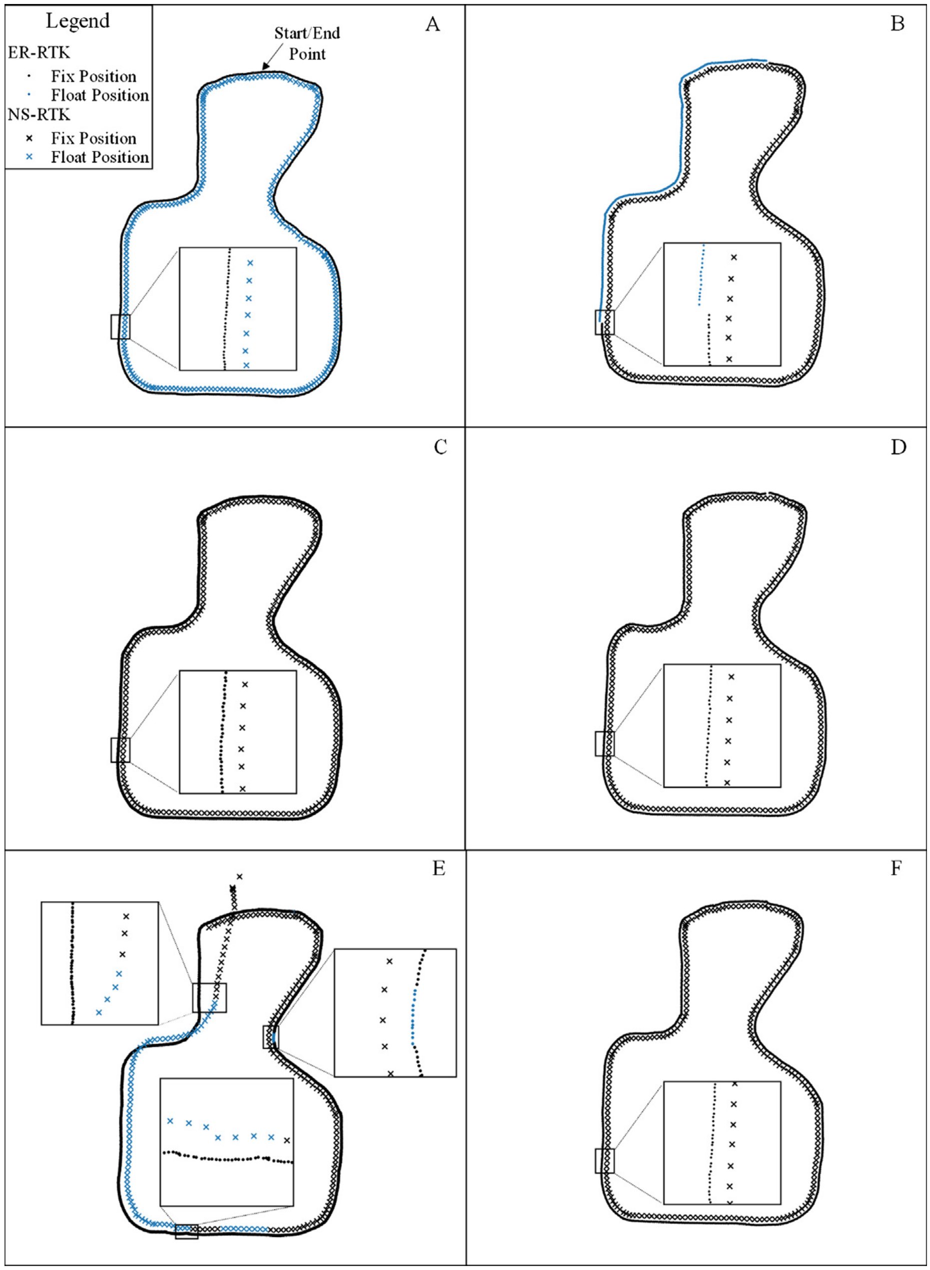

Fig. 6. Robot trajectories of the ER-RTK and NS-RTK GNSSs. Note that black symbols represent fixed solution status positions (expecting centimetre accuracy) and blue symbols float solution status positions (expecting sub-meter accuracy). (For interpretation of the references to colour in this figure legend, the reader is referred to the web version of this article.)

in fixed solution status, whereas this was the case in only 71.5% of the data for the NS-RTK.

To assess the combined accuracy of the two RTK-GNSSs, the constant physical distance between the ER-RTK and the NS-RTK antennas (472 mm) was used. It was assumed that if both GNSSs worked accurately, the distance obtained from the ER-RTK and NS-RTK data would be close to this reference distance. Table 4 shows the statistical analysis for the DEN and error (MAE and RMSE). For trial 3, 4 and 6, where all data were in fixed solution status, the mean distance between two antennas was found 477.9 mm, 479.8 mm, and 481.8 mm, respectively, all close to the reference distance of 472 mm. The root-mean-square distance error (RMSE) was 30.7 mm for trial 3, 33.6 mm for trial 4, and 32.2 mm for trial 6, which was within expected error limits. A moderately accurate result was obtained from trials 1 and 2. During trial 1, all NS-RTK data was in float solution status (blue crosses in Fig. 6A) and all ER-RTK data was in fixed solution status. Conversely, during trial 2, part of the ER-RTK data was in float solution status (blue dots in Fig. 6B) whereas all of the NS-RTK data was in fixed solution status. Therefore, it was expected that trial 2 would yield higher accuracy than trial 1, but the result was the opposite; in trial 1, the RMSE was 49.4 mm and, in trial 2 the RMSE was 122.7 mm. Nevertheless, since the accuracy of RTK GNSSs in float solution status is assumed at sub-meter level (Bakker et al., 2011; Bechar and Vigneault, 2017), the RMSE error for trials 1 and 2 are within expected limits. Trial 5 represents an outlier, since here the false fixed solution problem occurred; the RMSE of 1307.4 mm places it outside expected limits, even in the case of float solution status.

It is important to emphasize that the results shown in Table 4 were for both GNSS combined, since they are separated by 472 mm on the robot, which was the reference for calculating the combined accuracy. In this experiment, it was not possible to determine the accuracy for the NS-RTK and ER-RTK GNSSs separately, for lack of a higher accuracy

Table 3
Statistical analysis for Distances Travelled Per Second (DTPSs) for the NS-RTK and ER-RTK GNSS.

Trial	RTK GNSS	Mean (mm)	SD (mm)	Min (mm)	Max (mm)	CV (%)	TDT (mm)
1	NS-RTK	309.02a	164.38	1.00	577.64	53.20	95177.87
	ER-RTK	318.33a	162.69	0.00	581.10	51.11	98046.34
2	NS-RTK	467.10a	78.08	180.34	574.01	16.72	94821.13
	ER-RTK	481.81b	60.95	237.43	685.62	12.65	97808.04
3	NS-RTK	461.60a	71.74	157.18	581.01	15.54	94166.44
	ER-RTK	475.98b	57.45	234.69	582.02	12.07	97100.40
4	NS-RTK	449.50a	74.49	100.41	566.82	16.57	94845.16
	ER-RTK	461.71b	62.91	200.00	558.75	13.62	97419.98
5	NS-RTK	497.80a	381.78	108.69	5767.50	76.69	105533.16
	ER-RTK	462.06b	63.04	168.96	553.11	13.64	97957.26
6	NS-RTK	440.84a	71.05	183.17	550.36	16.12	94779.89
	ER-RTK	454.61b	59.71	197.09	556.18	13.14	97741.35
SDTDT (mm)	NS-RTK						4411.12a
	ER-RTK						356.31b
SDTDT* (mm)	NS-RTK						366.84a
	ER-RTK						368.03a

SD – Standard deviation, Min – Minimum, Max – Maximum, CV – Coefficient of Variation, TDT – Total Distance Travelled, SDTDT – Standard deviation for TDT, SDTDT – Standard deviation for TDT without considering trial 5. Different letters (a, b) in different rows (NS-RTK or ER-RTK) imply statistically significant different values based on an F-test.*

Table 4
Statistical analysis of the distance between the ER-RTK and NS-RTK GNSS antennas (DEN) and error (MAE and RMSE) being the difference between DEN and the true distance between both antennas (472 mm).

Trial	Mean (mm)	SD (mm)	Min (mm)	Max(mm)	CV (%)	MAE (mm)	RMSE (mm)
1	459.80	48.29	360.56	537.89	10.50	10.20	49.36
2	552.08	91.27	438.32	760.68	16.53	−82.08	122.75
3	477.94	29.70	429.56	526.85	6.21	−7.94	30.75
4	479.87	32.12	419.15	532.12	6.69	−9.78	33.57
5	1028.70	1182.02	433.05	5973.63	114.90	−558.70	1307.41
6	481.77	29.98	419.31	535.05	6.22	−11.77	32.20

SD – Standard deviation, Min – Minimum, Max – Maximum, CV – Coefficient of variation, MAE – Mean absolute distance error between two GNSSs and reference. RMSE – Root-mean-square distance error.*

GNSS.

Overall, the results imply that it is possible to use low-cost RTK GNSSs for ground robots that need high precision. The experiments show that a guidance system could be developed with two low-cost RTK GNSS rovers on a robot (Rovira-Más et al., 2015). To increase the system efficiency and reduce problems with RTK GNSS communication loss, low-cost RTK GNSS could also be fused by Kalman filtering with other sensors, such as LIDAR, Inertial Measurement Units (IMUs), cameras, and others (Dong et al., 2011; Hu and Uchimura, 2004; Ji et al., 2012; McKinion et al., 2010; Schleicher et al., 2010; Van Henten et al., 2003; Weiss and Biber, 2011; Xue et al., 2012; Yin and Noguchi, 2013).

4. Conclusions

Two robot borne low-cost Real-time Kinematic Global Navigation Satellite Systems (RTK GNSSs) being an Emlid “Reach” (ER-RTK) and a NavSpark “NS-HP” (NS-RTK) were evaluated in terms of precision and accuracy. Localization precision was evaluated by analysing the GNSS data collected during six trials where the robot was steered by remote control along a predefined path. When the RTK GNSS interprets data in fixed solution status, it can attain the highest precision and accuracy; in this status, the accuracy error expectation is less than 50 mm, whereas in float solution status the accuracy error expectation is less than 1 m.

Regarding all trials combined, fixed solution status was present among 94.0% of the data for the ER-RTK GNSS and 71.5% for the NS-RTK GNSS. The ER-RTK GNSS also attained higher precision than the NS-RTK GNSS during dynamic field tests; the average variation among the six trials in the Total Distance Travelled (TDT) by the NS-RTK GNSS was approximately 4,411 mm compared to 356 mm for the ER-RTK GNSS.

During one of the six trials, a phenomenon termed false fixed solution was encountered; here, the RTK GNSS claims it has attained a high-accuracy fixed position, but, in reality, it has not. This type of error is not uncommon in low-cost single-frequency RTK GNSSs and are typically caused by interference, multipath errors and noise. Adjusting the RTK receiver’s parameters can alleviate this to a certain extent. Discarding the trial where the false fixed solution occurred resulted in similar precision for both low-cost RTK systems. Although more research is needed to address this issue, false fixed solution status may be alleviated by sensor fusion with alternative guidance instruments such as Inertial Measurement Units (IMUs) through Kalman filtering.

Overall, the data showed that both tested low-cost RTK GNSSs have potential for use in experimental guidance systems in agriculture and beyond.

Declaration of Competing Interest

All authors are aware of the ethics policy of the Computers and Electronics in Agriculture Journal, declare no conflict of interest and accept responsibility for the present manuscript.

Appendix A. Supplementary material

Supplementary data to this article can be found online at https://doi.org/10.1016/j.compag.2019.105142.

References

Bakker, T., van Asselt, K., Bontsema, J., Müller, J., van Straten, G., 2011. Autonomous navigation using a robot platform in a sugar beet field. Biosyst. Eng. 109, 357–368. https://doi.org/10.1016/j.biosystemseng.2011.05.001.

Bechar, A., Vigneault, C., 2017. Agricultural robots for field operations. Part 2: Operations and systems. Biosyst. Eng. 153, 110–128. https://doi.org/10.1016/j.biosystemseng.2016.11.004.

Bechar, A., Vigneault, C., 2016. Agricultural robots for field operations: concepts and components. Biosyst. Eng. 149, 94–111. https://doi.org/10.1016/j.biosystemseng.2016.06.014.

Dabove, P., Manzino, A.M., 2017. Artificial neural network for detecting incorrectly fixed phase ambiguities for L1 mass-market receivers. GPS Solut. 21, 1213–1219. https://doi.org/10.1007/s10291-017-0605-x.

Dong, F., Heinemann, W., Kasper, R., 2011. Development of a row guidance system for an autonomous robot for white asparagus harvesting. Comput. Electron. Agric. 79, 216–225. https://doi.org/10.1016/j.compag.2011.10.002.

Dong, F., Petzold, O., Heinemann, W., Kasper, R., 2013. Time-optimal guidance control for an agricultural robot with orientation constraints. Comput. Electron. Agric. 99, 124–131. https://doi.org/10.1016/j.compag.2013.09.009.

Hu, Z.H.Z., Uchimura, K., 2004. Real-time data fusion on tracking camera pose for direct visual guidance. IEEE Intell. Veh. Symp. 2004, 842–847. https://doi.org/10.1109/IVS.2004.1336494.

Ji, W., Zhao, D., Cheng, F., Xu, B., Zhang, Y., Wang, J., 2012. Automatic recognition vision system guided for apple harvesting robot. Comput. Electr. Eng. 38, 1186–1195. https://doi.org/10.1016/j.compeleceng.2011.11.005.

Koo, G., Kim, K., Chung, J., Choi, J., Kwon, N.-Y., Kang, D.-Y., Sohn, H., 2017. Development of a high precision displacement measurement system by fusing a low cost RTK-GPS sensor and a force feedback accelerometer for infrastructure monitoring. Sensors 17, 2745. https://doi.org/10.3390/s17122745.

Liu, T., Li, B., 2017. Single-frequency BDS/GPS RTK with low-cost U-blox receivers. pp. 232–238.

McKinion, J.M., Willers, J.L., Jenkins, J.N., 2010. Comparing high density LIDAR and medium resolution GPS generated elevation data for predicting yield stability. Comput. Electron. Agric. 74, 244–249. https://doi.org/10.1016/j.compag.2010.08.011.

Morimoto, E., Suguri, M., Umeda, M., 2005. Vision-based navigation system for autonomous transportation vehicle. Precis. Agric. 6, 239–254. https://doi.org/10.1007/s11119-005-1384-x.

Mousazadeh, H., 2013. A technical review on navigation systems of agricultural autonomous off-road vehicles. J. Terramech. 50, 211–232. https://doi.org/10.1016/j.jterra.2013.03.004.

Odolinski, R., 2017. Low-cost , 4-system , precise GNSS positioning : a GPS , Galileo , BDS and QZSS ionosphere-weighted RTK analysis.

Odolinski, R., Teunissen, P.J.G., 2017. Low-cost, high-precision, single-frequency GPS–BDS RTK positioning. GPS Solut. 21, 1315–1330. https://doi.org/10.1007/s10291-017-0613-x.

Oksanen, T., Backman, J., 2013. Guidance system for agricultural tractor with four wheel steering. IFAC Proc. Vol. (IFAC-PapersOnline) IFAC. https://doi.org/10.3182/20130327-3-JP-3017.00030.

Pedersen, S.M., Fountas, S., Have, H., Blackmore, B.S., 2006. Agricultural robots – system analysis and economic feasibility. Precis. Agric. 7, 295–308. https://doi.org/10.1007/s11119-006-9014-9.

Perez-Ruiz, M., Slaughter, D.C., Gliever, C., Upadhyaya, S.K., 2012. Tractor-based Real-time Kinematic-Global Positioning System (RTK-GPS) guidance system for geospatial mapping of row crop transplant. Biosyst. Eng. 111, 64–71. https://doi.org/10.1016/j.biosystemseng.2011.10.009.

Rovira-Más, F., Chatterjee, I., Sáiz-Rubio, V., 2015. The role of GNSS in the navigation strategies of cost-effective agricultural robots. Comput. Electron. Agric. 112, 172–183. https://doi.org/10.1016/j.compag.2014.12.017.

Schleicher, D., Bergasa, L.M., Ocaña, M., Barea, R., López, E., 2010. Low-cost GPS sensor improvement using stereovision fusion. Signal Process. 90, 3294–3300. https://doi.org/10.1016/j.sigpro.2010.05.017.

Subramanian, V., Burks, T.F., Arroyo, A.A., 2006. Development of machine vision and laser radar based autonomous vehicle guidance systems for citrus grove navigation. Comput. Electron. Agric. 53, 130–143. https://doi.org/10.1016/j.compag.2006.06.001.

Takasu, T., Ebinuma, T., Yasuda, A., 2009. Effect of Quasi Zenith Satellite (QZS) on GPS positioning 2. Simulation and evaluation, pp. 2–6.

Takasu, T., Yasuda, A., 2013. RTKLIB ver. 2.4.2 Manual 181.

Takasu, T., Yasuda, A., 2009. Development of the low-cost RTK-GPS receiver with an open source program package RTKLIB. In: Int. Symp. GPS/GNSS, pp. 4–6.

Tsakiri, M., Sioulis, A., Piniotis, G., 2017. Compliance of low-cost, single-frequency GNSS receivers to standards consistent with ISO for control surveying. Int. J. Metrol. Qual. Eng. 8, 11. https://doi.org/10.1051/ijmqe/2017006.

Valbuena, R., Mauro, F., Rodriguez-Solano, R., Manzanera, J.a, 2010. Accuracy and precision of GPS receivers under forest canopies in a mountainous environment. Spanish J. Agric. Res. 8, 1047–1057. https://doi.org/10.5424/sjar/2010084-1242.

Van Henten, E.J., Van Tuijl, B.A.J., Hemming, J., Kornet, J.G., Bontsema, J., Van Os, E.A., 2003. Field test of an autonomous cucumber picking robot. Biosyst. Eng. 86, 305–313. https://doi.org/10.1016/j.biosystemseng.2003.08.002.

Weiss, U., Biber, P., 2011. Plant detection and mapping for agricultural robots using a 3D LIDAR sensor. Rob. Auton. Syst. 59, 265–273. https://doi.org/10.1016/j.robot.2011.02.011.

Xue, J., Zhang, L., Grift, T.E., 2012. Variable field-of-view machine vision based row guidance of an agricultural robot. Comput. Electron. Agric. 84, 85–91. https://doi.org/10.1016/j.compag.2012.02.009.

Yin, X., Noguchi, N., 2013. Development of a target following system for a field robot. IFAC Proc. 4, 109–114. https://doi.org/10.3182/20130828-2-SF-3019.00068.